City Research Online

City, University of London Institutional Repository

Vortex formation and recirculation zones in left anterior descending artery stenoses: computational fluid dynamics analysis

D G Katritsis[1,4], A Theodorakakos[2], I Pantos[1,3], A Andriotis[2], E P Efstathopoulos [3], G Siontis[4], N Karcanias[5], S Redwood[4] and M Gavaises [5]

Short Title: Flow in LAD stenoses

[1] Department of Cardiology, Athens Euroclinic, Athens, Greece

[2] Fluid Research, Athens, Greece

[3] 2nd Department of Radiology, Medical School, University of Athens, Greece

[4] Cardiothoracic Unit, St Thomas' Hospital, London, UK

[5] School of Engineering and Mathematical Sciences, The City University, London, UK

Correspondence:

D. Katritsis, PhD

Department of Cardiology,

Athens Euroclinic,

9 Athanassiadou Str., 115 21 Athens, Greece

Tel 210 6416600, Fax: 210 6416530,

e-mail: dkatritsis@euroclinic.gr and dgkatr@otenet.gr

Abstract

Flow patterns may affect the potential of thrombus formation following plaque rupture. Computational fluid dynamics (CFD) were employed to assess hemodynamic conditions, and particularly flow recirculation and vortex formation in reconstructed arterial models associated with ST elevation myocardial infraction (STEMI) or stable coronary stenosis (SCS) in the left anterior descending coronary artery (LAD). Results indicate that in the arterial models associated with STEMI, a 50% diameter stenosis immediately before or after a bifurcation creates a recirculation zone and vortex formation at the orifice of the bifurcation branch, for most of the cardiac cycle, thus allowing the creation of stagnating flow. These flow patterns are not seen in the SCS model with an identical stenosis. Post-stenotic recirculation in the presence of a 90% stenosis was evident at both the STEMI and SCS models. The presence of 90% diameter stenosis resulted in flow reduction in the LAD of 51.5 % and 35.9 % in the STEMI models, and 37.6% in the SCS model, for a 10 mmHg pressure drop. CFD simulations in reconstructed model of stenotic LAD segments indicate that specific anatomic characteristics create zones of vortices and flow recirculation that promote thrombus formation and potentially myocardial infarction.

1.Introduction

Intracoronary ultrasound studies have suggested that plaque rupture itself may not necessarily lead to clinical events (Hong *et al.*, 2004; Maehara *et al.*, 2002; Rioufol *et al.*, 2002). A high incidence of multiple plaque ruptures remote from the culprit lesion been reported in patients with acute coronary syndromes (ACS) (Hong et al., 2004), and plaque ruptures have also been identified in patients with stable angina or asymptomatic ischemia (Maehara et al., 2002). Therefore, vulnerable plaque rupture may be a frequent event that only occasionally leads to ACS. It has been suggested that it is not the composition of the plaque, i.e. the size of the underlying lipid pool or necrotic core that leads to post-plaque rupture thrombus formation and ACS, but rather the thrombogenicity of the resulting cavity (Fujii et al., 2003). Mechanical and flow parameters may contribute to plaque rupture and subsequent thrombosis in this respect. There has been evidence that platelet deposition is correlated to flow patterns like flow separation, and recirculation (Bluestein *et al.*, 1997; Raz *et al.*, 2007). However, the potential effect of local hemodynamic factors on thrombus formation in the coronary arterial tree is not known.

We have previously shown that a combination of specific anatomic parameters predispose to vulnerable plaque development, rupture of the plaque and consequent thrombosis (Katritsis *et al.*, 2008; Katritsis *et al.*, 2009). In the present study we hypothesized that at sites of coronary artery occlusion, hemodynamic conditions such as flow recirculation predispose to development of occlusive thrombus formation and ST elevation myocardial infarction (STEMI). Computational fluid dynamics (CFD) simulations were employed for assessment of flow characteristics and particularly vortex formation and recirculation in models reconstructing segments of the left anterior descending artery (LAD) with STEMI-related occlusion or stable stenosis.

2. Materials and Methods

2.1 Geometric Models

Geometric models of coronary arteries were obtained from previous analyses of patients who presented with an anterior STEMI and had a patent LAD, either due to thrombolysis or spontaneous

recanalization, at time of angiography. Angiograms of patients with stable coronary stenoses (SCS) and a significant LAD stenosis were reconstructed in the three-dimensional (3D) space and analyzed for the provision of control geometric models. Details of our methodology that aimed at ensuring as much representative models as possible have been published elsewhere (Katritsis et al., 2009). In brief, angiograms were obtained in standard projections and diastolic images from two "perpendicular views" (view angulation greater than 30°) were 3-D reconstructed in the study core laboratory (Coronary Flow Research Unit at Athens Euroclinic). Three-dimensional reconstruction was accomplished with the use of a reconstruction algorithm developed by our group (Andriotis et al., 2008).

The following geometric features of coronary lesions were extracted from the reconstructed arterial trees: lesion length, distance of most stenotic site from the ostium of LAD, LAD reference diameter and LAD curvature at the lesion site. The following features regarding bifurcation branches were also extracted for all proximal and distal to the lesion bifurcations: distance of the bifurcation from the most stenotic site, bifurcation take-off angle and bifurcation diameter at its orifice. This analysis provided detailed quantitation of all geometric features of the reconstructed arterial trees. Details and data derived have been previously presented (Katritsis et al., 2009). A bifurcation branch was considered to be on the culprit lesion if its orifice was between the proximal and distal non diseased segments of the artery. The geometric features of 19 cases of STEMI with a bifurcation on the lesion before the site of maximum stenosis were averaged to obtain a representative geometry designated as STEMI 1. Accordingly, the geometric features of 27 cases of STEMI with a bifurcation on the lesion after the site of maximum stenosis and 35 cases of SCS without bifurcations on the lesion were averaged and designated as STEMI 2 and SCS respectively. These three averaged representative geometries were selected as coronary models to be further studied in CFD simulations in order to evaluate hemodynamic conditions in respect to flow circulation at critical areas. The geometric features of the three models are described in table 1. For each model three cases were considered: an unrestricted model and three models with increasing degree of diameter stenosis of 20%, 50% and 90% (Figure 1). The rationale was to evaluate flow conditions in both tight and non-significant stenoses since vulnerable plaques are often associated with positive arterial remodeling that results in

angiographically subcritical lesions. The studied coronary models were considered stationary and the vessel walls were considered rigid.

2.2 CFD Analysis

Numerical grids for twelve total cases were constructed with tetrahedral and wedge elements (Figure 2) using the commercial grid generator software Gambit. Each numerical grid consisted of approximately 2 million cells with varying grid density. Denser grid notes have been placed near the wall boundary of the arterial tree as well as at the bifurcation points. Simulations have been also performed with lower/higher number of cells in order to make sure that with the number of cells finally adopted for the parametric study, grid independency has been achieved.

The in-house CFD flow solver (GFS) has been used in this study (Giannadakis *et al.*, 2008; Strotos *et al.*, 2008; Theodorakakos *et al.*, 2008; Tonini *et al.*, 2008). The fluid model solves numerically the time averaged form of the full Navier-Stokes equations describing the laminar or turbulent motion of a fluid using fully unstructered numerical grids. These equations are written for an arbitrary coordinate system and for cartesian velocity components as follows:

Mass conservation equation:

$$\frac{\partial \rho}{\partial t} + \nabla \cdot \rho \vec{u} = 0 \qquad (1)$$

where ρ is the density, t the time, $\vec{u}$ the velocity vector.

Momentum conservation equation:

$$\frac{\partial \rho \vec{u}}{\partial t} + \nabla \cdot \left(\rho \vec{u} \otimes \vec{u} - \overline{S} \right) = 0$$

$$\qquad (2)$$

$$\overline{S} = -\left(P + \frac{2}{3}\mu\nabla \cdot \vec{u} \right)\overline{I} + \mu\left(\nabla \otimes \vec{u} + \left(\nabla \otimes \vec{u} \right)^{T} \right)$$

and $\overline{S}$ the stress tensor, P the pressure, μ the viscosity of the fluid and $\overline{I}$ is the unit tensor. The discretisation method is based on the finite volume approach and the pressure is computed with a method resembling the PISO algorithm (Bressloff, 2001; Issa, 1986); a 2nd order spatial discretisation scheme has been used. For simulating non-Newtonian fluid flow, different models for the molecular viscosity can be found in literature. Shibeshi and Collins have shown that blood at rest requires a yield

stress to start flowing (Shibeshi and Collins, 2005). The power law does not take into account this characteristic feature. The Casson model, however, takes into consideration this behavior of blood, and that was the reason that this model was chosen to be used in the present study. In this model the blood viscosity is given by the equation:

$$\mu = \frac{\tau_0}{\dot{\gamma}} + \frac{\sqrt{\eta \cdot \tau_0}}{\sqrt{\dot{\gamma}}} + \eta \quad (3)$$

where τ_0 is the yield stress and η is the Casson rheological constant (Johnston et al., 2004). Widely accepted values for those constants are 0.005 Pa for τ_0 and 0.0035 Pa•s for η (Bressloff, 2001). The maximum value for the viscosity used is 0.01 Pa•s (Shibeshi and Collins, 2005). Furthermore, $\dot{\gamma}$ is the shear rate. The relation between $\dot{\gamma}$ and the rate of deformation $\overline{D}$ is expressed as:

$$\dot{\gamma} = \sqrt{\frac{1}{2} \cdot \sum_i \sum_j \left(D_{ij} \cdot D_{ji}\right)} \quad (4)$$

The rate of deformation tensor $\overline{D}$ can be expressed as:

$$\overline{D} = \frac{1}{2} \cdot \left[\nabla \otimes \vec{u} + \left(\nabla \otimes \vec{u}\right)^T\right] \quad (5)$$

The shear stress tensor $\overline{\tau}$ is related to viscosity μ and the rate of deformation $\overline{D}$ according to the relation:

$$\overline{\tau} = \mu \cdot \overline{D} \quad (6)$$

At the inlet, a pre-described pulse of the blood flow rate and pressure has been assumed (Berne and Levy, 2001); (Figure 2) and corresponds to a typical flow rate variation during the cardiac cycle. At the walls, no slip condition is applied. For the conditions at the exit of each branch, again the mass flow rate is prescribed using the following procedure which can be realized schematically in Figure 2. A total pressure drop is assumed for the whole arterial system which includes the known geometry in which the flow will be simulated and the remaining unknown fluid circuit. Two known geometries are considered. The first one represents a non-stenotic artery while the second is the actual geometry with the stenosis. For arterial trees without stenosis arteries typically adapt to maintain a normal WSS

through a compensatory mechanism (Glagov S et al., 1998). The WSS for laminar steady flow in a

straight tube may be estimated by the following equation:

$$\tau_{wall} = \frac{32 \cdot \mu \cdot Q}{\pi \cdot D^3} \qquad (7)$$

where Q is the volumetric flow rate, µ is the blood viscosity and D is the conduit diameter. Thus the

volumetric flow rate through each branch can be assumed to be analogous to the third power of the

conduit diameter D. In order to estimate the percentage of flow rate that enters each branch after a

bifurcation, the following procedure is employed, similar to that proposed by Chen et al (Chen et al.,

2005). First, the vessel's diameters are measured just before and after the bifurcation. Then, the

pressure drop in each of the branches present in the unrestricted geometric model can be estimated

while at the same time the pressure drop in the remaining unknown flow circuit present at the end of

the branches considered can be computed by a simple subtraction from the assumed total pressure

head. That allows estimation of the flow resistance in the unknown circuit. This flow resistance of the

unknown circuit is then assumed to be the same also for the restricted arterial tree. Steady-state

calculations are then performed for the restricted arterial tree using the same total pressure drop values

but at the same time knowing the flow resistance of the unknown arterial circuit. An iterative process

is employed in which the flow for each branch is recalculated so that the total pressure drop remains

the same. That eventually leads to a reduced total flow rate due to the increased pressure drop that the

stenosis causes. Since the method cannot be employed for pulsatile pressure input, during the time

steps of the transient flow simulation the pressure drop through each branch is linearly interpolated

from the values obtained from the steady-state simulations. A large number of 36 cases have been

simulated for obtaining the flow rate distribution in each of the branches considered in the

reconstructed arterial trees, for different pressure drops and different degrees of stenoses.

2.3 Quantitation of Flow Patterns

For quantifying the expected variations between the geometries investigated, two parameters were

plotted: (i) the total flow rate reduction induced by the stenosis relative to that of the unrestricted

arterial tree, in each branch considered, and (ii) the temporal variation of area blockage percentage of

each branch along the length of every arterial tree. This parameter is calculated on cross sections

normal to the branch direction and along its length and it is defined as the percentage of area having

velocity vectors facing in the direction opposite to the flow exit. It can be interpreted as the percentage

of cross sectional area blocking the flow through it due to the formation of a recirculation zone. It has

to be further noted that the value of this coefficient is smaller than the actual equivalent diameter of

the recirculation zone. The latter is not possible to be defined here due to the 3-D shape of the

simulated vessels; however, for axisymmetric sudden contraction geometries the area of the

recirculation zone can be approximately 1.5 times larger than the blockage area as defined here.

3. Results

3.1 Flow distribution

3.1.1 No Significant Stenosis. Figure 3 shows the flow distribution inside the STEMI 1 case for the

unrestricted geometry and the one with the 20% stenosis, respectively; the time instance corresponds

to normalised time of approximately 0.75 which, as can be seen in Figure 2, is the time of the peak

flow rate through the simulated geometry. It can be seen that for the unrestricted geometry, even at the

maximum flow rate, no major recirculation is formed along the main branch as well as at the entry to

the bifurcation branches considered. When a small degree of stenosis is introduced, a weak

recirculation starts to appear to the entry of branch 3, at selective time instances. Still, this is very

weak and appears only occasionally.

3.1.2 Significant Stenosis. Figure 4 shows a close-up picture of flow recirculation at the orifice of

branch 3 for the STEMI 1 case by introducing a 50% stenosis on the main branch. Restricting the flow

downstream of the bifurcation point results in the formation of a strong recirculation zone. Such vortex

formation is also present for the STEMI 2 but not for the SCS geometry. Analysis of the flow lines

over the whole cardiac cycle indicates that for most of the cardiac cycle, the flow is not significantly

affected for this geometry. This is fundamentally different from the flow distribution developing

within the STEMI 1 and 2 geometries. More severe flow recirculations are formed with increasing

degree of stenosis on the main branch. Figure 5 refers to the 90% stenosis of the STEMI 2 geometry. It can be seen that the flow is practically blocked not only to the entry of branch 3, but also just downstream of the stenosis along the main branch. The 90% stenosis case causes severe flow recirculation not only on the STEMI 1 and 2 cases but this time also in the post-stenotic lumen of the SCS model.

3.2 Quantitative Analysis of Recirculation and Flow Reduction

Table 2 shows the percentage of inflow reduction relative to that of the unrestricted arterial tree for the 50 and 90% degree of stenosis, respectively, for all three groups of geometries considered for the two total pressure drops of 10 and 20mm of Hg. All 50% stenosis cases result only to a very small reduction of the fluid quantity flowing through the whole arterial tree. The 90% stenosis results in a significant variation, which still is not proportional to the introduced area reduction. The flow distribution of individual branches reveals that immediately after the stenosis the LAD lumen and the adjacent bifurcation branch (branch 3) exhibit a significant flow reduction, up to 80% in comparison with the unrestricted case (table 2).

Figure 6 shows contour plots of the non-dimensional time history of the area blockage percentage along their normalised length for the various cases considered and specific branches. This percentage can be interpreted as the percentage of cross sectional area of the vessel occupied by flow recirculation, thus it is quantitative measure of the restriction induced flow recirculation. All contour plots show a horizontal low value zone at around normalised time 0.4. This feature is attributed exclusively to pre-described blood flow conditions and not to coronary anatomy. Indeed, this time corresponds to the time instant where the flow used as input for the simulations reverses direction. The fact that it covers the whole length of the branch is due to the boundary conditions used, which consider incompressible fluid and rigid wall arteries; as a result, when negative flow is pre-specified as input, the flow distribution is affected almost in the whole arterial tree.

The upper panel of Figure 6 refers to branch 3 of STEMI 1, STEMI 2, and SCS, respectively, using the 50% stenosis while the corresponding results for the 90% cases are shown in the middle panel of

Figure 6. The results indicate that at the initial part of branch 3 and up to a dimensional length of 1.5 mm, a recirculation zone is present for most of the cardiac cycle. The blockage levels can be as low as 30%, implying that more than 70% of the flow area is occupied by a recirculation zone. This circulation is stronger for the case of 50% stenosis of the STEMI 1 geometry; similar levels are also calculated for the 90% stenosis of the STEMI 2 arterial tree configuration. Thus, although the flow rate reduction through that branch for the 50% stenosis is not very significant compared to the unrestricted case, the actual liquid velocity distribution allows for the formation of a relatively large area where the flow stagnates; the implication of that may be critical compared to the SCS geometry where such a behaviour is not observed as can be seen in the same figures.

Similar sets of results for the main branch are presented in the lower panel of Figure 6, for the 90% stenosis case and for all three groups of geometries. The turning of the flow into the first bifurcation, which is found approximately at a normalised distance of 0.2, results to some flow recirculation. A strong recirculation zone however, is found after the stenosis. There, blockage values can be as low as 30% for all three groups for almost the whole cardiac cycle, indicating similar flow behaviour with respect to flow stagnation independently of the position of the bifurcations in relation to the point of maximum stenosis.

4. Discussion

Thrombus formation is thought to begin with an event such as plaque rupture or vessel damage, resulting in the exposure of active tissue factor on the vessel wall (Fuster et al., 1992). To attract and bind platelets to injured or malfunctioning endothelium, the von Willebrand factor (vWf), a long chain molecule, mediates the interaction between platelets and a vascular lesion (Goto et al., 1995; Ikeda et al., 1997). Platelets have various receptors for vWf, some of which are activated by mechanical stimuli, such as high shear stress. Individual platelets adhere to altered vascular surfaces and are activated, after which the integrin IIb-IIIa can bind plasma proteins, notably fibrinogen, vWF and fibronectin; these adhesive substrates immobilized on the membrane surface then recruit additional platelets, resulting in aggregation and thrombus growth (Ruggeri, 2002). The relationship of hemodynamic factors and thrombus formation due to platelet deposition has been previously

investigated in various experimental and computational CFD studies (Bluestein *et al.*, 1997; Raz *et al.*, 2007; Pivkin *et al.*, 2006; Miyazaki and Yamaguchi, 2003). These studies showed that slowly recirculating flow due to core jet flow patterns through a stenosis promote aggregation of platelets and platelet-activating factors. Also, blood stagnation occurring at areas with disturbed flow may facilitate the accumulation of blood thrombogenic factors close to the wall (Feldman et al., 2002). Since adhesion of platelets to a surface is greatly enhanced by prior activation (Wurzinger et al., 1985), this mechanism offers an explanation for the increased platelet deposition at the recirculation zone: platelets that are already activated by the high shear stresses at the throat and along the shear layer between the jet and the slowly recirculating vortices, are brought into contact by the contracting streamlines on the slower side of this shear layer. Once trapped in the recirculation zone, the motion of the platelets along the curved streamlines with components perpendicular to the wall bring them into contact with the wall along the reattachment point and the slowly recirculating flow adjacent to the wall (Wurzinger et al., 1985). Formation of vortices has been also associated with the presence of side branches under pulsating flow conditions similar to those of coronary circulation (Chakravarty and Sen, 2008). The results of these previous studies indicate that thrombus formation after atheromatic plaque rupture is promoted by vortex formation due to recirculating flow.

Our study provides evidence that specific anatomic features of the coronary structure at the vicinity of atherosclerotic plaque are related to vortex formation. If the hemodynamic conditions at the vicinity of a plaque are favourable, then potential plaque rupture would lead to occlusive thrombus formation and subsequent myocardial infarction. This might partially explain why many plaques along the coronary tree rupture but few lead to myocardial infarction due to occlusive thrombus formation. Results indicate that in all cases of our study when a non significant arterial stenosis is introduced, recirculation starts to appear at the orifice of the pre-stenotic arterial branch although it is weak and evident only at selective time instances. This observation is in line with previous evidence (Chakravarty and Sen, 2008). However when the diameter stenosis becomes 50%, there is evident differentiation between models with and without a post-stenotic bifurcation, since a strong recirculation zone is formed at the orifice of the post-stenotic bifurcation branch whereas flow is not significantly affected in the absence of bifurcation. This phenomenon may possibly be relevant to

thrombus formation since post-stenotic flow conditions favour platelet aggregation, particularly when previously activated by the elevated shear stresses of the stenotic region. The observation that myocardial infarctions often occur at sites of mild-to-moderate stenoses (Ambrose *et al.*, 1988; Little *et al.*, 1988) could be considered in this context. Minor plaques creating non-significant stenoses might be prone to rupture with a subsequent creation of mild to moderate obstruction that given the right hemodynamic conditions might lead to thrombosis. When these conditions are not met, ruptured plaques do not evolve into coronary occlusions. When stenosis severity increases, flow recirculation is also increasing. In extremely tight stenosis (90% in our study), flow is practically blocked just downstream of the stenosis along the main branch due to severe recirculation, even in the absence of a bifurcation. This suggests that even if a presumably stable coronary lesion becomes extremely tight it can lead to thrombotic occlusion after plaque rupture. This observation is also in keeping with previous evidence that significant, complex lesions are prone to develop total occlusions (Kaski et al., 1995) and postmortem examinations demonstrating that ruptured plaques leading to acute coronary syndrome more likely occur within the segment of significant stenosis (Falk, 1983; Qiao and Fishbein, 1991; Richardson *et al.*, 1989).

According to our model, the presence of bifurcations creates vortexes mainly at the ostium of the side branch. Therefore, since the recirculation zone of vortex shedding causes platelet aggregation there, one might expect the thrombosis to occur in the arterial branch, not the parent artery. However, the post mortem pathology of fatal infarctions may show thrombus within the ruptured plaque itself regardless of branching patterns. A plausible explanation for this phenomenon is that post-MI, when no recanalization occurs, as was the case in our patients from whom the experimental coronary models were derived, the side branch on the infarct site usually gets thrombosed, and thus renders itself non-identifiable, or subtotally occluded. Thus, thrombosis might start at the ostium of the side branch and extend towards the main branch where it causes the major infarct.

The presence of bifurcations may also predispose to the development of myocardial infarction via diverse mechanisms. Bifurcating branches along the main coronary arteries have been shown to cause flow disturbances and alter local hemodynamic conditions that favor both the development of atherosclerosis and plaque vulnerability (Theodorakakos *et al.*, 2008; Asakura and Karino, 1990;

Papafaklis *et al.*, 2007; Soulis *et al.*, 2006). Atherosclerotic lesions are known to develop at specific regions, such as arterial curvatures and bifurcations, where disturbed flow and conditions of low or even oscillatory shear stress initially occur (Iwami *et al.*, 1998; VanderLaan *et al.*, 2004). Low shear stress induces lesions with a vulnerable plaque phenotype and creates the condition for plaque rupture and subsequent thrombosis even in non-significant stenosis (Cheng *et al.*, 2006; Chatzizis *et al.*, 2008). In addition, a highly localized circumferential wall stress concentration of approximately 9 to 14 times the proximal circumferential wall stress occurs at bifurcation sites (Salzar et al., 1995), which undergo a larger deformation during cyclic flexion of the coronary artery, yielding a higher circumferential stress than those further to bifurcations (Wu et al., 2003).

5. Study limitations

Models of arterial segment reconstruction were derived from specific anatomic patterns identified in the LAD of patients with an anteroseptal STEMI. STEMI, however, can also be seen with different anatomic conditions. Thus, our results cannot be generalized for all STEMI settings. The STEMI lesions are examined after the plaque rupture and MI so these lesions would likely look different if examined before the STEMI. In our models all lesions were assumed to be axisymmetric whereas asymmetric coronary lesions are frequently observed. Unfortunately, in humans it is not possible to identify and study culprit coronary segments, that develop thrombotic occlusion, before the actual event. At the inlet a typical pulse of the blood flow rate and pressure during the cardiac cycle has been assumed. Finally, the studied coronary segments were considered only at diastole and thus stationary, and the vessel walls were considered rigid.

6. Conclusion

CFD predictions indicate that flow disturbances and particularly flow recirculation and vortex formation caused by stenotic lesions of the left anterior descending coronary artery are not identical in models derived from arterial segments with thrombotic occlusion or stable lesions. Specific anatomic conditions identified at sites of coronary occlusions, such as the presence of bifurcation branches,

create local hemodynamic conditions that promote thrombus formation and may affect the clinical outcome of coronary plaque rupture.

References

Ambrose J A, Tannenbaum M A, Alexopoulos D, Hjemdahl-Monsen C E, Leavy J, Weiss M, Borrico S, Gorlin R and Fuster V 1988 Angiographic progression of coronary artery disease and the development of myocardial infarction *Journal of the American College of Cardiology* **12** 56-62

Andriotis A, Zifan A, Gavaises M, Liatsis P, Pantos I, Theodorakakos A, Efstathopoulos E P and Katritsis D 2008 A new method of three-dimensional coronary artery reconstruction from X-ray angiography: validation against a virtual phantom and multislice computed tomography *Catheter Cardiovasc Interv* **71** 28-43

Asakura T and Karino T 1990 Flow patterns and spatial distribution of atherosclerotic lesions in human coronary arteries *Circ Res* **66** 1045-66

Berne R M and Levy M N 2001 *Cardiovasular Physiology* (St. Louis, USA: Mosby Inc)

Bluestein D, Niu L, Schoephoerster R T and Dewanjee M K 1997 Fluid mechanics of arterial stenosis: relationship to the development of mural thrombus *Annals of biomedical engineering* **25** 344-56

Bressloff N W 2001 A parallel pressure implicit splitting of operators algorithm applied to flows at all speeds *Int. J. Numer. Methods Fluids* **36** 497-518

Chakravarty S and Sen S 2008 Analysis of pulsatile blood flow in constricted bifurcated arteries with vorticity-stream function approach *Journal of medical engineering & technology* **32** 10-22

Chatzizisis Y S, Jonas M, Coskun A U, Beigel R, Stone B V, Maynard C, Gerrity R G, Daley W, Rogers C, Edelman E R, Feldman C L and Stone P H 2008 Prediction of the localization of high-risk coronary atherosclerotic plaques on the basis of low endothelial shear stress: an intravascular ultrasound and histopathology natural history study *Circulation* **117** 993-1002

Chen M C, Lu P C, Chen J S and Hwang N H 2005 Computational hemodynamics of an implanted coronary stent based on three-dimensional cine angiography reconstruction *Asaio J* **51** 313-20

Cheng C, Tempel D, van Haperen R, van der Baan A, Grosveld F, Daemen M J, Krams R and de Crom R 2006 Atherosclerotic lesion size and vulnerability are determined by patterns of fluid shear stress *Circulation* **113** 2744-53

Falk E 1983 Plaque rupture with severe pre-existing stenosis precipitating coronary thrombosis. Characteristics of coronary atherosclerotic plaques underlying fatal occlusive thrombi *British heart journal* **50** 127-34

Feldman C L, Ilegbusi O J, Hu Z, Nesto R, Waxman S and Stone P H 2002 Determination of in vivo velocity and endothelial shear stress patterns with phasic flow in human coronary arteries: a methodology to predict progression of coronary atherosclerosis *American heart journal* **143** 931-9

Fujii K, Kobayashi Y, Mintz G S, Takebayashi H, Dangas G, Moussa I, Mehran R, Lansky A J, Kreps E, Collins M, Colombo A, Stone G W, Leon M B and Moses J W 2003 Intravascular ultrasound assessment of ulcerated ruptured plaques: a comparison of culprit and nonculprit lesions of patients with acute coronary syndromes and lesions in patients without acute coronary syndromes *Circulation* **108** 2473-8

Fuster V, Badimon L, Badimon J J and Chesebro J H 1992 The pathogenesis of coronary artery disease and the acute coronary syndromes (2) *The New England journal of medicine* **326** 310-8

Giannadakis E, Gavaises M and Arcoumanis C 2008 Modelling Cavitation in Diesel Injector Nozzle Holes *J. Fluid Mechanics* **616** 153-93

Glagov S, Zarins C, Giddens DP and DN K 1998 Hemodynamics and atherosclerosis: insights and perspectives gained from studies of human arteries *ArchPatholLabMed* **112** 1018-31

Goto S, Salomon D R, Ikeda Y and Ruggeri Z M 1995 Characterization of the unique mechanism mediating the shear-dependent binding of soluble von Willebrand factor to platelets *The Journal of biological chemistry* **270** 23352-61

Hong M K, Mintz G S, Lee C W, Kim Y H, Lee S W, Song J M, Han K H, Kang D H, Song J K, Kim J J, Park S W and Park S J 2004 Comparison of coronary plaque rupture between stable angina and acute myocardial infarction: a three-vessel intravascular ultrasound study in 235 patients *Circulation* **110** 928-33

Ikeda Y, Murata M and Goto S 1997 Von Willebrand factor-dependent shear-induced platelet aggregation: basic mechanisms and clinical implications *Annals of the New York Academy of Sciences* **811** 325-36

Issa R I 1986 Solution of implicitly discretised fluid flow equations by operator-splitting *Journal of Computational Physics* **62** 40-65

Iwami T, Fujii T, Miura T, Otani N, Iida H, Kawamura A, Yoshitake S, Kohno M, Hisamatsu Y, Iwamoto H and Matsuzaki M 1998 Importance of left anterior descending coronary artery curvature in determining cross-sectional plaque distribution assessed by intravascular ultrasound *The American journal of cardiology* **82** 381-4

Johnston B M, Johnston P R, Corney S and Kilpatrick D 2004 Non-Newtonian blood flow in human right coronary arteries: steady state simulations *Journal of biomechanics* **37** 709-20

Kaski J C, Chester M R, Chen L and Katritsis D 1995 Rapid angiographic progression of coronary artery disease in patients with angina pectoris. The role of complex stenosis morphology *Circulation* **92** 2058-65

Katritsis D G, Efstathopoulos E P, Pantos J, Korovesis S, Kourlaba G, Kazantzidis S, Marmarelis V and Voridis E 2008 Anatomic characteristics of culprit sites in acute coronary syndromes *Journal of interventional cardiology* **21** 140-50

Katritsis D G, Pantos I, Korovesis S, Hadjipavlou M, Tzanalaridou E, Lockie T, Redwood S, Voridis E and Efstathopoulos E P 2009 Three-dimensional analysis of vulnerable segments in the left anterior descending artery *Coronary artery disease*

Little W C, Constantinescu M, Applegate R J, Kutcher M A, Burrows M T, Kahl F R and Santamore W P 1988 Can coronary angiography predict the site of a subsequent myocardial infarction in patients with mild-to-moderate coronary artery disease? *Circulation* **78** 1157-66

Maehara A, Mintz G S, Bui A B, Walter O R, Castagna M T, Canos D, Pichard A D, Satler L F, Waksman R, Suddath W O, Laird J R, Jr., Kent K M and Weissman N J 2002 Morphologic and angiographic features of coronary plaque rupture detected by intravascular ultrasound *Journal of the American College of Cardiology* **40** 904-10

Miyazaki H and Yamaguchi T 2003 Formation and destruction of primary thrombi under the influence of blood flow and von Willebrand factor analyzed by a discrete element method *Biorheology* **40** 265-72

Papafaklis M I, Bourantas C V, Theodorakis P E, Katsouras C S, Fotiadis D I and Michalis L K 2007 Association of endothelial shear stress with plaque thickness in a real three-dimensional left main coronary artery bifurcation model *International journal of cardiology* **115** 276-8

Pivkin I V, Richardson P D and Karniadakis G 2006 Blood flow velocity effects and role of activation delay time on growth and form of platelet thrombi *Proceedings of the National Academy of Sciences of the United States of America* **103** 17164-9

Qiao J H and Fishbein M C 1991 The severity of coronary atherosclerosis at sites of plaque rupture with occlusive thrombosis *Journal of the American College of Cardiology* **17** 1138-42

Raz S, Einav S, Alemu Y and Bluestein D 2007 DPIV prediction of flow induced platelet activation-comparison to numerical predictions *Annals of biomedical engineering* **35** 493-504

Richardson P D, Davies M J and Born G V 1989 Influence of plaque configuration and stress distribution on fissuring of coronary atherosclerotic plaques *Lancet* **2** 941-4

Rioufol G, Finet G, Ginon I, Andre-Fouet X, Rossi R, Vialle E, Desjoyaux E, Convert G, Huret J F and Tabib A 2002 Multiple atherosclerotic plaque rupture in acute coronary syndrome: a three-vessel intravascular ultrasound study *Circulation* **106** 804-8

Ruggeri Z M 2002 Platelets in atherothrombosis *Nature medicine* **8** 1227-34

Salzar R S, Thubrikar M J and Eppink R T 1995 Pressure-induced mechanical stress in the carotid artery bifurcation: a possible correlation to atherosclerosis *Journal of biomechanics* **28** 1333-40

Shibeshi S and Collins W 2005 The Rheology of Blood Flow in a Branched Arterial System *Appl Rheol* **15** 398-405

Soulis J V, Giannoglou G D, Chatzizisis Y S, Farmakis T M, Giannakoulas G A, Parcharidis G E and Louridas G E 2006 Spatial and phasic oscillation of non-Newtonian wall shear stress in human left coronary artery bifurcation: an insight to atherogenesis *Coronary artery disease* **17** 351-8

Strotos G, Gavaises M, Theodorakakos A and Bergeles G 2008 Parametric Investigation on the Evaporation of Droplets Depositing on Heated Surfaces at Low Weber Numbers *Int. J. Heat and Mass Transfer* **51** 1516-29

Theodorakakos A, Gavaises M, Andriotis A, Zifan A, Liatsis P, Pantos I, Efstathopoulos E P and Katritsis D 2008 Simulation of cardiac motion on non-Newtonian, pulsating flow development in the human left anterior descending coronary artery *Physics in medicine and biology* **53** 4875-92

Tonini S, Gavaises M and Theodorakakos A 2008 Modelling of High Pressure Dense Diesel Sprays with Adaptive Local Grid Refinement, Part I: Numerical Implementation *Int. J. Heat and Fluid Flow* **29** 427-48

VanderLaan P A, Reardon C A and Getz G S 2004 Site specificity of atherosclerosis: site-selective responses to atherosclerotic modulators *Arteriosclerosis, thrombosis, and vascular biology* **24** 12-22

Wu H C, Chen S Y, Shroff S G and Carroll J D 2003 Stress analysis using anatomically realistic coronary tree *Medical physics* **30** 2927-36

Wurzinger L J, Blasberg P and Schmid-Schonbein H 1985 Towards a concept of thrombosis in accelerated flow: rheology, fluid dynamics, and biochemistry *Biorheology* **22** 437-50
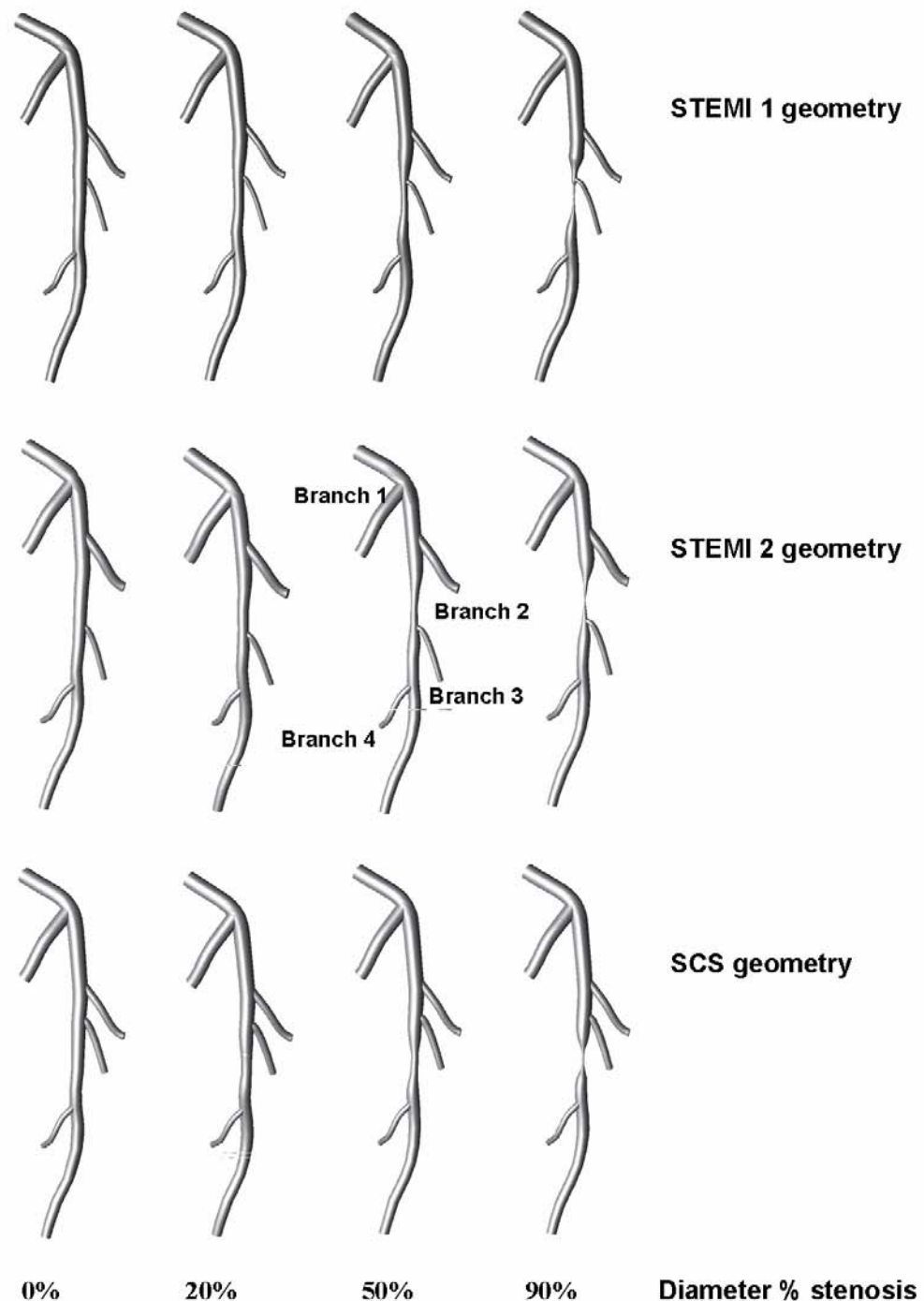
Figure 1. Simplified, three-dimensional arterial models of representative 3-D anatomic geometries derived from analysis of angiograms from all patients in the myocardial infarction (STEMI) and stable coronary artery stenosis (SCS) groups, with varying degree of diameter % stenosis (no stenosis, 20%, 50% and 90%). On-lesion bifurcation before and after culprit plaque were seen mainly in patients with STEMI, and lesion without bifurcation were seen mainly in patients with SCS.
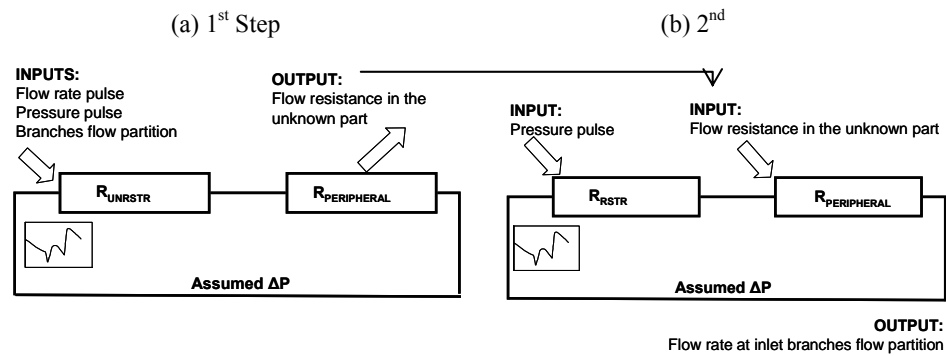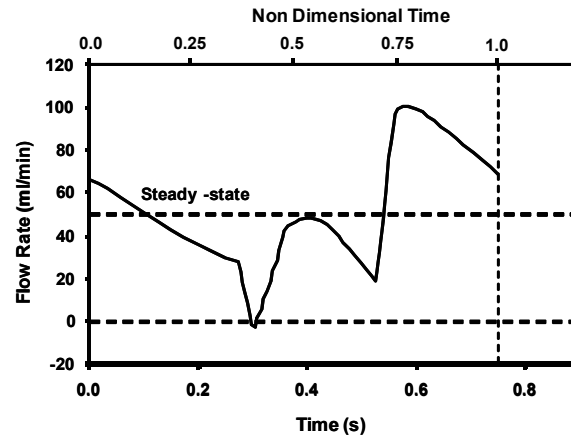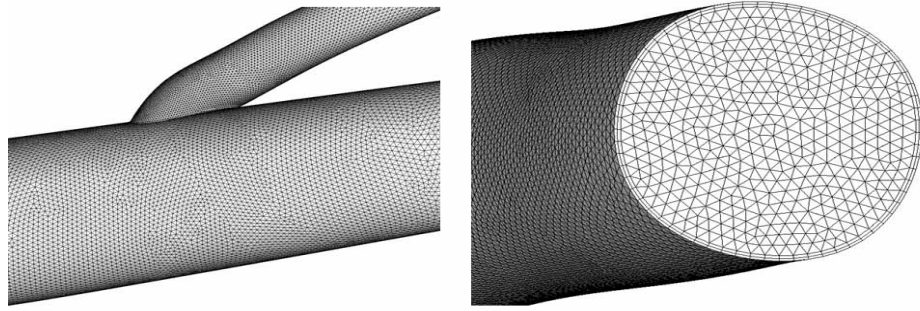
Figure 2.

Upper panel: Details of the numerical grid

Middle panel: Phasic coronary blood flow rate used as input for the arterial tree.

Lower panel: Schematic diagram of the equivalent electric circuit of pressure losses (a) in the unrestricted and (b) the restricted geometry. R_{UNRSTR} is the flow resistance in the simulated arterial branch without the stenosis, R_{RSTR} is the flow resistance in the simulated arterial branch with the stenosis and $R_{PERIPHERAL}$ is the flow resistance of the remaining blood flow circuit for an assumed ΔP (steady state simulations for assumed ΔP 10 and 20 mm Hg).
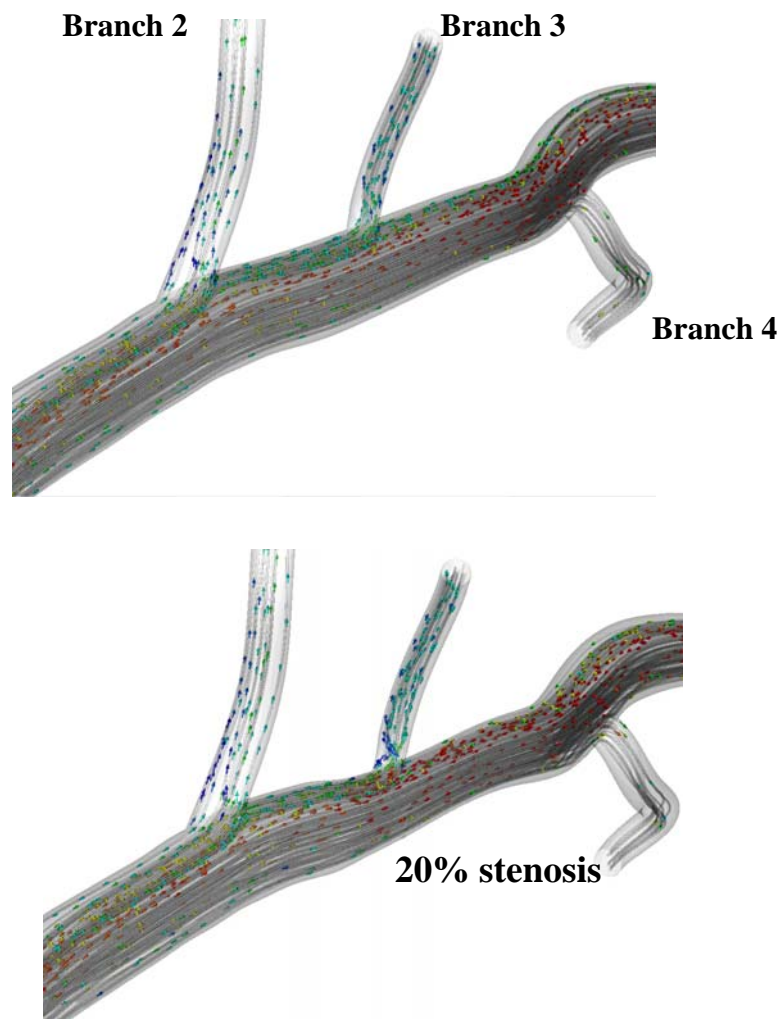
STEMI 1

Figure 3. Flow distribution in STEMI 1 geometry at normalised time 0.75, which corresponds to maximum flow rate, for a normal lumen (upper panel) and a 20% stenosis (lower panel). No recirculation zones are noted.

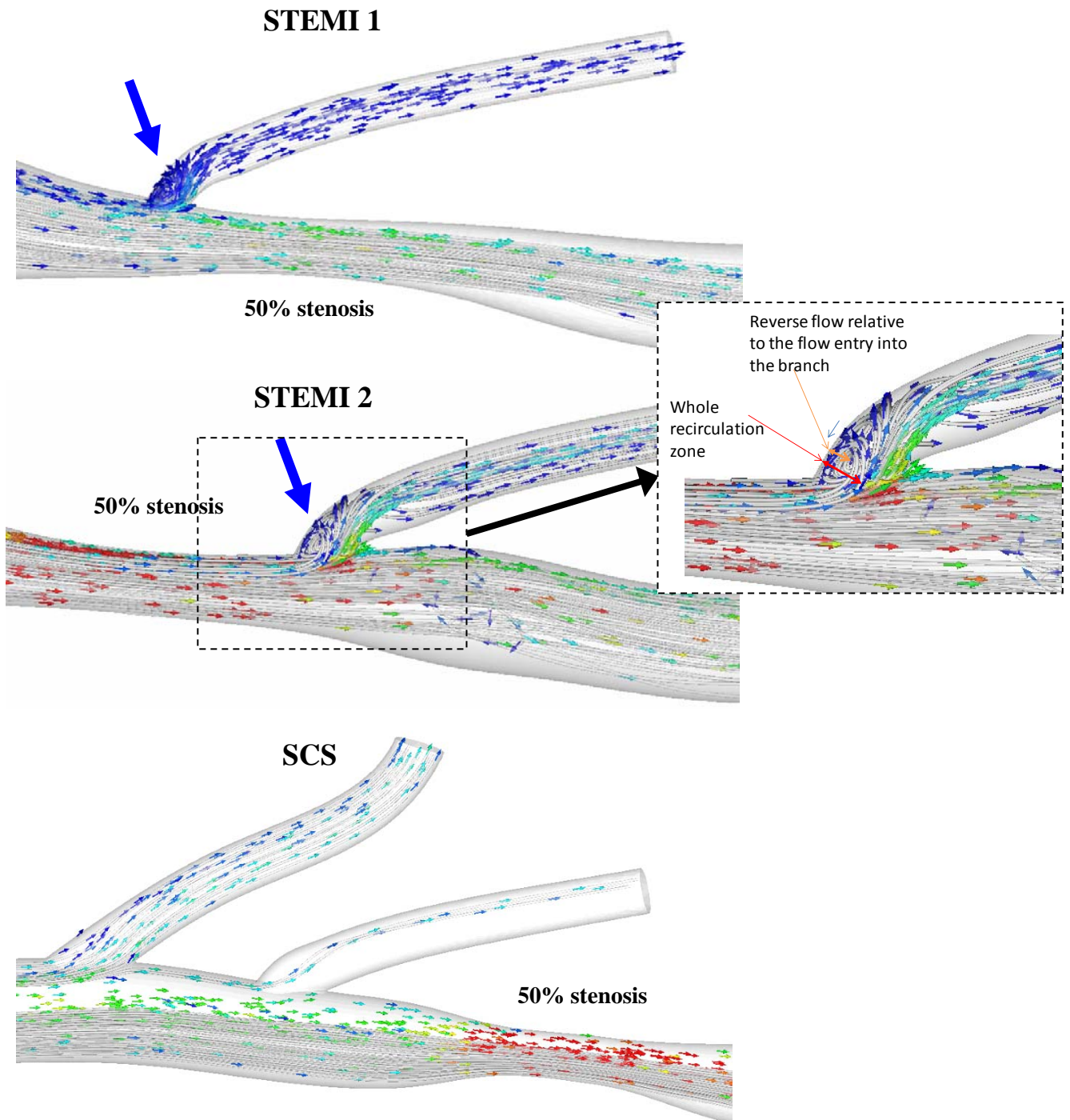STEMI: ST-elevation myocardial infarction.

Figure 4. Typical flow distribution for geometries with 50% diameter stenosis investigated at normalised time 0.5. There is flow recirculation at the ostium of the side branch in both STEMI geometries (blue arrows) whereas no recirculation is seen at the SCS model. In STEMI 2 geometry the recirculation vortex virtually blocks the entry to the branch (details in the enlarged image).

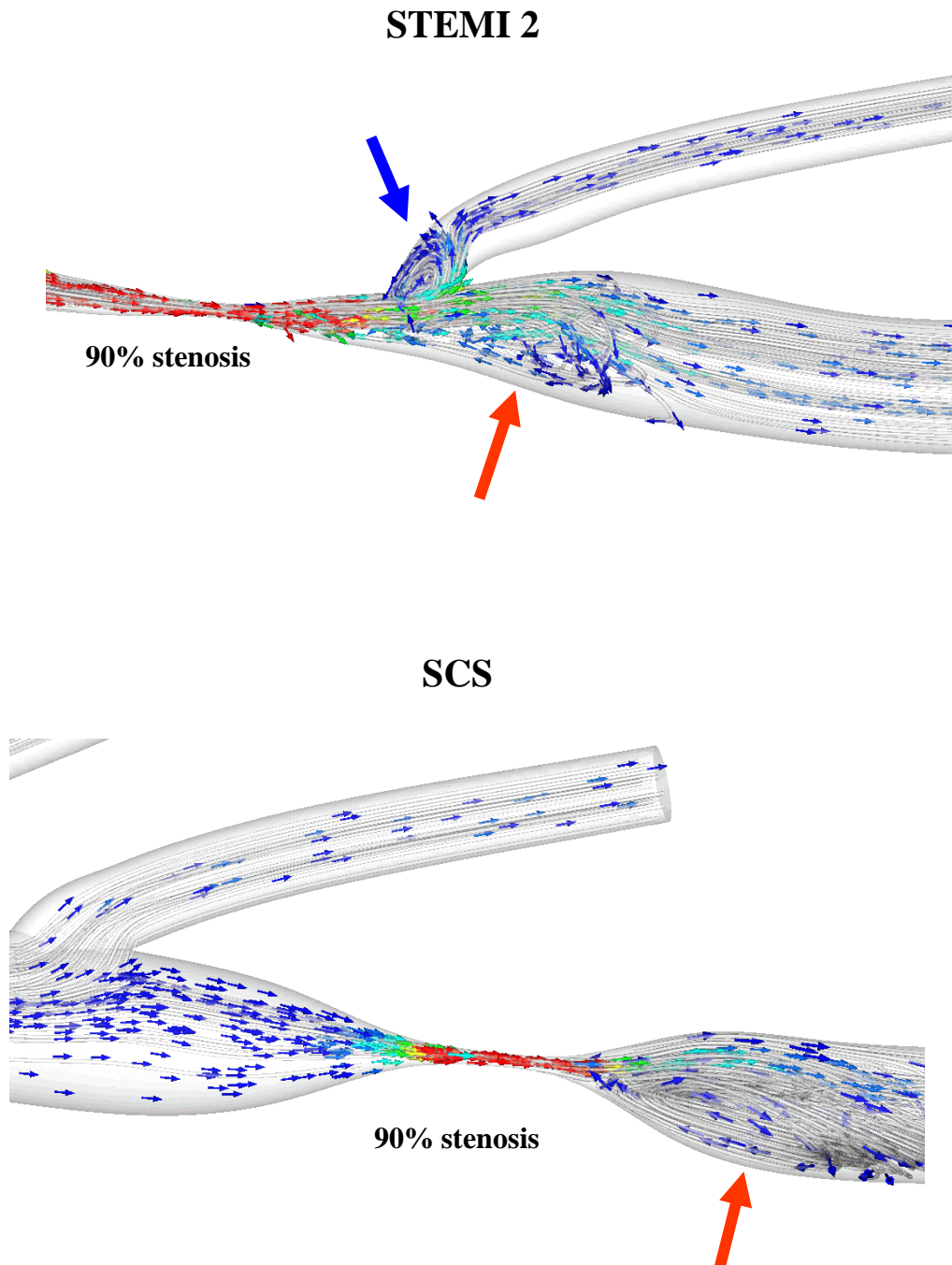STEMI: ST-elevation myocardial infarction, SCS: stable coronary stenosis.

STEMI 2

SCS

Figure 5. Typical flow distribution for geometries with 90% diameter stenosis investigated at normalised time 0.5. In the STEMI 2 geometry flow recirculation occurs in both main (red arrow) and side branch (blue arrow) after the stenosis. In the SCS geometry recirculation is also seen in the post-stenotic lumen of the main branch (red arrow) despite the absence of bifurcation.

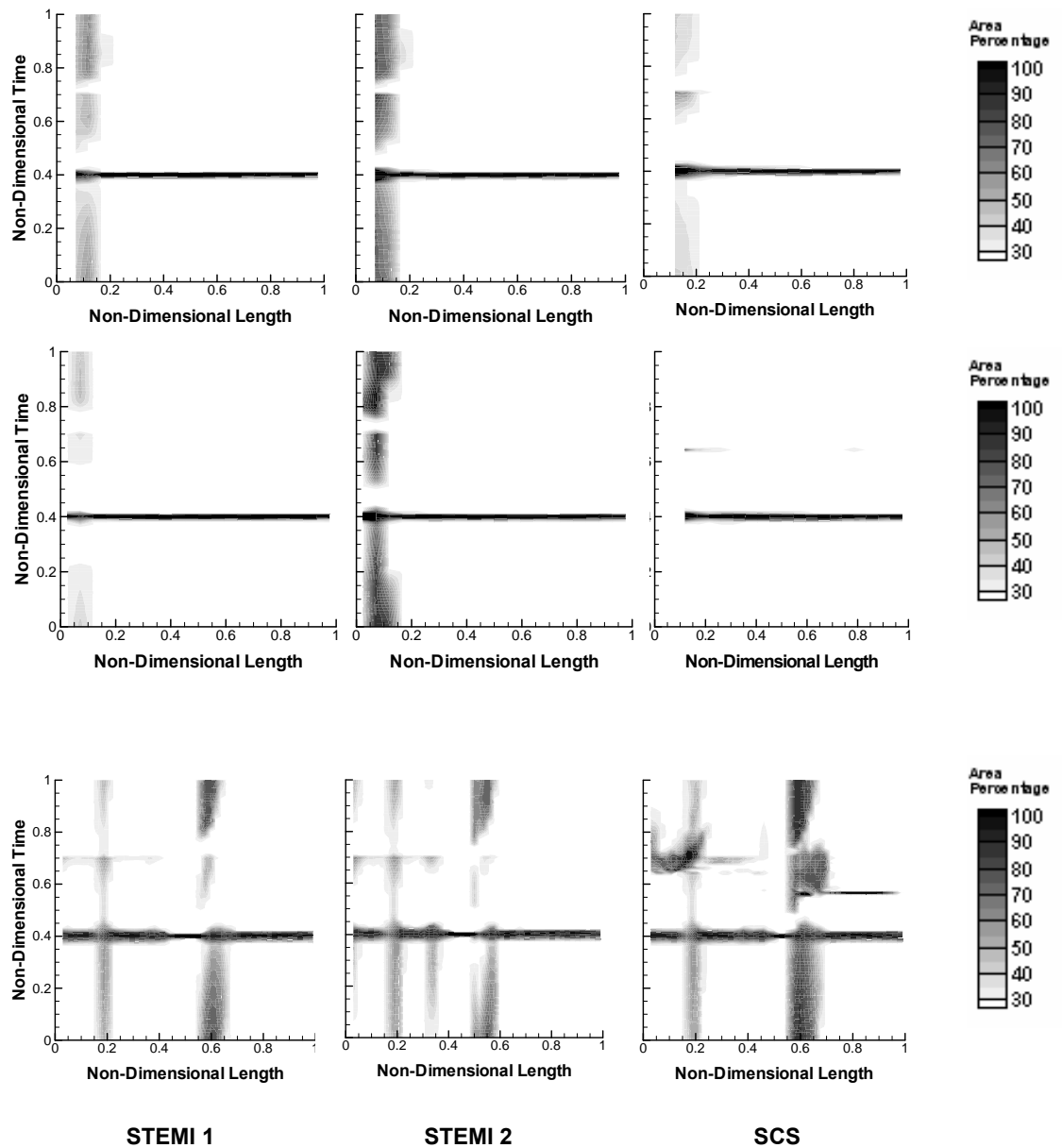STEMI: ST-elevation myocardial infarction, SCS: stable coronary stenosis.

Figure 6.

STEMI 1   STEMI 2   SCS

Upper Panel: Contour plot of the area blockage percentage time history along the length of branch 3, for the 50% stenosis case in STEMI 1, STEMI 2 and SCS geometry.

Middle Panel: Contour plot of the area blockage percentage time history along the length of branch 3, for the 90% stenosis case in STEMI 1, STEMI 2 and SCS geometry**.**

Lower Panel: Contour plot of the area blockage perecentage time history along the length of main branch for the 90% stenosis case in STEMI 1, STEMI 2 and SCS geometry. The vertical lines B1, B2, B3 and B4 indicate the locations of the 4 branches along the LAD while S indicates the location of maximum stenosis and t_1 and t_2 correspond to the time of minimum flow rate of Figure 2b.

STEMI: ST-elevation myocardial infarction, SCS: stable coronary stenosis.

Tables

Table 1. Averaged geometric features for the three most prevalent angiographic settings.

	STEMI 1 n=19	STEMI 2 n=27	SCS n=35
Lesion length (mm)	19.0	16.1	9.7
Lesion reference diameter (mm)	3.0	3.0	2.7
Side branch 1 diameter (mm)	2.9	3.3	3.0
Side branch 1 take-off angle (^{o})	79	86	80
Side branch 2 diameter (mm)	1.9	2.2	1.6
Side branch 2 take-off angle (^{o})	60	82	80
Side branch 3 diameter (mm)	1.4	1.5	1.5
Side branch 3 take-off angle (^{o})	60	73	80
Side branch 4 diameter (mm)	1.4	1.4	1.2
Side branch 4 take-off angle (^{o})	62	70	75
Side branch 1 – side branch 2 distance (mm)	20.4	12.7	17.8
Side branch 2 – side branch 3 distance (mm)	14.1	n/a	8.5
Side branch 2 – most stenotic site distance (mm)	n/a	17.2	n/a
Side branch 3 – most stenotic site distance (mm)	4.1	n/a	10.1
Most stenotic site – side branch 3 distance (mm)	n/a	4.0	n/a
Most stenotic site – side branch 4 distance (mm)	20.3	n/a	13.7
Side branch 3 – side branch 4 distance (mm)	n/a	17.8	n/a
Angulation on lesion (^{o})	154	151	163

STEMI: ST-elevation myocardial infarction

SCS: stable coronary stenosis

n/a: not applicable

Table 2. Inflow reduction (percentage) relative to the inflow of the unrestricted arterial tree for the 50% and 90% stenoses for all three cases and two pressure drops (~0 indicates negligible change).

		STEMI 1 geometry				STEMI 2 geometry				SCS geometry			
		Total inflow	Branch 3	Branch 4	Outflow	Total inflow	Branch 3	Branch 4	Outflow	Total inflow	Branch 3	Branch 4	Outflow
50 % stenosis	10 mm Hg	2.4	1.1	3.9	3.8	~0	~0	~0	~0	0.8	~0	1.6	1.7
	20 mm Hg	1.2	0.6	2.0	2.0	~0	~0	~0	~0	0.4	~0	0.8	0.9
90 % stenosis	10 mm Hg	51.5	0.4	85.2	84.6	35.9	81.6	81.2	81.1	37.6	~0	84.4	84.3
	20 mm Hg	46.7	0.5	77.1	76.7	33.1	74.9	74.8	74.8	34.3	~0	77.0	76.8